Large-amplitude pulse response at the plasma boundary in an ion-beam system

T. Nagasawa and Y. Nishida
Department of Electrical and Electronic Engineering, Utsunomiya University, Utsunomiya, Tochigi 321, Japan
(Received 7 September 1993; revised manuscript received 10 December 1993)

The reflection and transmission of a plane ion-acoustic soliton from a steep density gradient in front of a sheath have been investigated experimentally in an ion pulse beam system. An incident pulse tunnels through the space-charge sheath area without time delay and separates into three pulses at the plasma-sheath boundary. These pulses consist of a reflected and two transmitted pulses. One of them is a pulse of a fast ion-beam mode, while the others are ion-acoustic waves. The model for interpreting the phenomena is discussed.

PACS number(s): 52.35.Sb, 52.35.Mw

I. INTRODUCTION

Experimental and theoretical studies of the reflection and transmission of plane ion-acoustic solitons from and through the plasma boundary have been performed by many researchers. Aksornkittiet *et al.* [1] and Schott [2] have shown the reflection of linear ion-acoustic waves for the mesh reflector. Dahiya, John, and Saxena [3] have shown the reflection of an ion-acoustic solitary wave from the nonuniform plasma density. They claimed that the reflection occurs from the sharp density gradient, the scale size of which is of the same order or even smaller than the initial wave width. Ishihara *et al.* [4] have suggested that long-wavelength waves are reflected before they reach the supersonic flow region within a sharp density gradient region in front of the electrode, where shock formation can absorb short-wavelength waves which are of the same order or even smaller than the initial wave width. Nishida [5] has pointed out that the reflection coefficient for the metallic disk or insulator sheet reflector depends on the sheath thickness in front of the reflector, and its coefficient is smaller than it for the metallic mesh reflector. Popa and Oeltl [6] have shown the efficient reflection properties of an ion-acoustic wave or soliton using a bipolar potential structure, and Raychaudhuri *et al.* [7] have proposed that this reflection mechanism is the reexcitation structure which is produced by ion perturbation explained by Gabl and Lonngren [8]. Nakamura, Ito, and Koga [9] have shown that for the metal disk, reflection and excitation of an ion-acoustic waves of large amplitude are observed when the bias on the disk reflector is positive, but they become small when it is negative and the excited wave is same as outgoing wave observed by Cooney, Gavin, and Lonngren [10]. A nonlinear ion-acoustic soliton with large amplitude has been investigated [11,12] for clarifying reflection and transmission phenomena, and the authors have pointed out that these phenomena can be explained by the nonlinear Snell's law [11]. However, the mechanism of these phenomena is not completely understood yet. Nishida, Yoshida, and Nagasawa [13,14] have shown that an ion-acoustic soliton tunnels through the sheath area without time delay, and the wave is resonantly absorbed when $D \cong L$, where D is the spatial width of the wave and L the characteristic gradient scale length of the sheath in front of the reflector. Also, Nagasawa co-workers [15,16] have shown that an incident soliton splits into reflected and transmitted waves at the sheath edge, and the reflection and/or transmission coefficients are a function of the velocity ratio of the reflected and incident waves. These results can be compared with the theoretical results [17], showing fairly good agreement.

In this paper we wish to show the results of the experimental observation on the reflection and transmission of plane ion-acoustic solitons at a plasma boundary performed in the ion-pulse-beam system produced by large applied pulse voltage. The results show the evidence of the tunnel effect, such as found in Refs. [13] or [14], even in the ion-beam system. And this tunnel effect decreases as the velocity of the incident pulse increases.

The present paper is organized as follows. The experimental apparatus and conditions are shown in Sec. II, and the experimental results are given in Sec. III. The discussions are presented to give the interpretation of the tunneling physics in Sec. IV. Finally, all the results are summarized in Sec. V.

II. EXPERIMENTS

The experiments are performed in a double plasma device produced in a stainless-steel chamber, the wall of which is covered with many multidipole permanent magnets. A plane stainless-steel grid (150 mesh/inch) for the plasma separation is fixed (see Fig. 1). The copper mesh reflector (30×35 cm^2, 15 mesh/inch) is movable in its angle to change the incident angle of the wave onto the reflector, and the electrode can be biased from about -23 V (floating potential) through -200 V with respect to the grounded target chamber. The velocity of an ion beam injected into the target plasma from the driver plasma can be changed by V_d (bias voltages between two plasmas). The typical plasma parameters are the electron density $n_e = (2-5) \times 10^8$ cm^{-3}, the electron temperature $T_e = (1-3)$ eV, and the ion temperature $T_i = T_e/(10-12)$ eV, measured by the Faraday cup in an argon gas at a pressure of $P = (3-4) \times 10^{-4}$ Torr. The pulses are picked

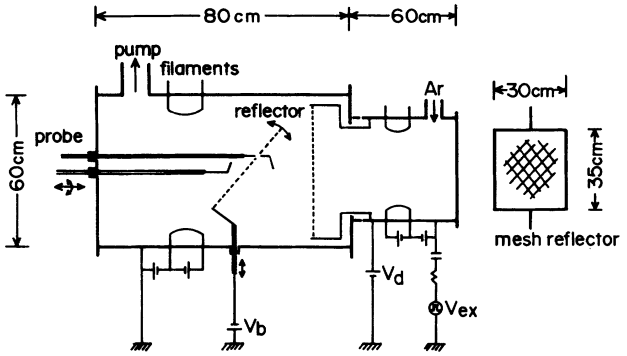

FIG. 1. Schematic of the experimental apparatus.

up by a cylindrical Langmuir probe (0.1-mm diameter by 1.0-mm length) which is biased slightly above the plasma potential in order to detect perturbations in the electron saturation current, and hence in the electron density. The signals are displayed on an oscilloscope screen, or analyzed with a boxcar integrator and recorded on an X-Y recorder.

A large-amplitude ion wave is excited by a double-plasma action, by applying a large positive pulse to the driver plasma. The shape of the pulse is a half of the sinusoidal wave, and its width is typically 10 μ sec.

III. EXPERIMENTAL RESULTS

Typical wave forms are shown in Fig. 2, where the incident pulse of the fast ion-beam mode denoted as W_{IB}, the reflected ion-acoustic pulse W_R, the transmitted pulse of the fast ion-beam mode W_{TB}, and a transmitted ion-acoustic pulse W_T are seen. The incident pulse is reflected at the sheath edge in front of the reflector, which is biased in deep negative voltages. After passing through the reflector, the transmitted pulse is split into two pulses, as also seen in the figure. Here $z<0$ is an incident side and $z>0$ corresponds to a transmission side.

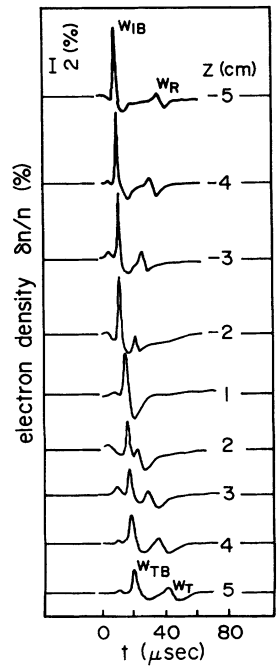

FIG. 2. Example of the propagation characteristics of the ion-beam pulses (W_{IB}, W_{TB}) and the ion-acoustic waves (W_R, W_T). $z>0$ stands for the incident side, and $z<0$ for the transmission side. The incident angle is $\theta_I=0°$, and the voltage on the reflector V_b is at a floating potential.

The loci of the maximum amplitude of each pulse are shown in Fig. 3. The velocity of the incident pulse corresponding to W_{IB} is $v_{IB}=4.9C_s$, $2.2C_s$, and $2.2C_s$, respectively, in Figs. 3(a), 3(b), and 3(c). The reflector for Figs. 3(a) and 3(b) is biased to the floating potential, and the incident angle for both cases are 0°. In the case of Fig. 3(c), the bias voltages on the reflector are -160 V. Here C_s is an ion-acoustic speed. As seen from Figs. 3(a) and 3(b), the time shift ($\Delta\tau$) between two pulses produced at the sheath area becomes larger as the velocity of the incident pulse becomes smaller, i.e., the incident pulse is shifted to an earlier time than that expected from the incident time delay at the sheath area. This means that the time delay within the sheath becomes negligibly small as the pulse velocity is smaller. The reflected pulse W_R is produced at the sheath edge, while the transmitted pulse appears at the sheath edge in the opposite side of the reflector, and this pulse splits into two pulses. One of them, denoted W_T, propagates with smaller velocity than the incident pulse, while the other, denoted W_{TB}, has a faster speed and it is almost the same speed as that of the incident ion-beam pulse. In Fig. 3(a), the velocity of W_R is $v_R=0.2v_{IB}=0.95C_s$, $v_T=0.14v_{IB}=0.68C_s$ for W_T, and $v_{TB}=v_{IB}=4.9C_s$ for W_{TB}. In Fig. 3(b), the velocity for each pulse is $v_R=0.33v_{IB}=0.73C_s$, $v_T=0.22v_{IB}=0.5C_s$, and $v_{TB}=0.94v_{IB}=2.1C_s$, respectively. Consequently, we can see that the velocity of the reflected pulse becomes larger as the velocity of the incident pulse becomes larger. One of the transmitted pulses has also the same character, but the other transmitted pulse W_{TB} has nearly the same velocity as the incident pulse. When the bias voltage on the reflector becomes deeply negative, the sheath width formed in front of the reflector becomes larger, and the points of the reflection and/or transmission are away from the reflector electrode, resulting in the time shift ($\Delta\tau$) becoming larger, as shown in Fig. 3(c). However, the velocity of each pulse in the uniform plasma area does not change with the bias voltages on the reflector.

The change of the amplitude of each pulse is shown in Figs. 4(a) and 4(b) as a function of the distance, z, measured from the reflector. In Fig. 4(a), the incident pulse observed in the beam mode decreases its amplitude as the pulse approaches the reflector, while other pulses attenuate as they propagate away from the reflector. Here, the beam velocity in this example is 8.5×10^5 cm/sec. The empirical relationship is given by the equation

$$\frac{\partial n}{n}=\alpha z^{-P}, \tag{1}$$

with $p=0.43$–0.48 for W_{TB}, $p=0.8$ for W_R, and $p=0.62$ for W_T, respectively, and α is constant. From

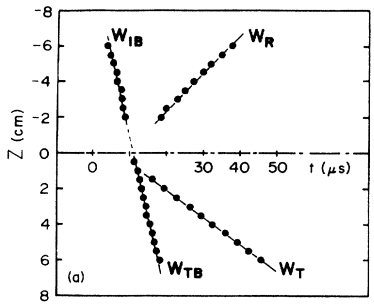

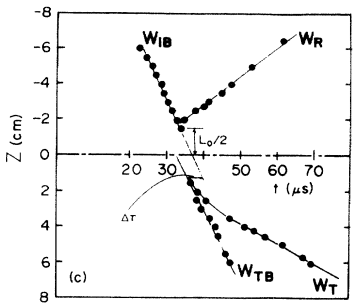

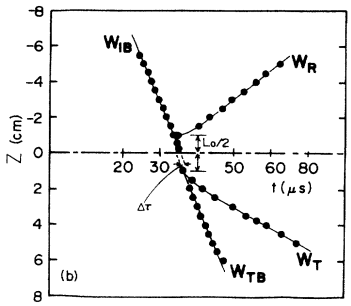

FIG. 3. Loci of the maximum amplitude. (a) The velocity v_{IB} of the incident pulse W_{IB} is $v_{IB}=4.9C_s$, and V_b is the floating potential. (b) $v_{IB}=2.2C_s$, and V_b is the floating potential. (c) $v_{IB}=2.2C_s$, and $V_b=-160$ V. The reflector is located at $z=0$ and $\theta_I=0°$.

these results, we can see that the damping rate of the transmitted pulse of the beam mode is smaller than those of other pulses. The reflected pulse has the largest damping rate of all the pulses. When the incident pulse W_I is a soliton with large amplitude, as is shown in Fig. 4(b), $p=0.44$ for W_T and $p=0.1$ for W_R. As seen in Fig. 4(b), the amplitudes of the transmitted pulses are larger than the reflected ones. This character is different from that of the beam mode shown in Fig. 4(a).

The dependence of the reflection γ_R and transmission coefficients γ_T on the reflector voltages is shown in Fig. 5. As the bias voltages V_b on the reflector become deep negative, the coefficient for the transmission of the ion-beam mode W_{TB} decreases, while those of pulses W_T and W_R increase.

The reflection and transmission coefficients of the ion-beam mode W_{TB} as a function of the incident pulse amplitude is shown in Fig. 6(a) as a parameter of the bias voltages on the reflector. When the bias voltages become deeply negative, the transmission coefficient decreases, but the reflection coefficient increases. The differences in the magnitude of these coefficients with parameter variation become smaller as the incident pulse amplitude becomes larger. In all these cases, the velocity of the incident pulse is kept constant at $v_{IB}=6.3C_s$. Figure 6(b) shows the case of the soliton being injected. As seen from this figure, the reflection and transmission coefficients show an inverse character compared with the case of the beam mode [Fig. 6(a)]. In the case of the reflection coefficient, no difference appears for the bias voltages on the reflector. Here the incident angle is kept constant $\theta_I=0°$.

Figure 7 shows the reflection coefficient γ_R or the transmission coefficient γ_T of the pulses W_R and W_{TB}, W_T as a function of the incident angle θ_I to the reflector. The transmission coefficient of W_{TB} increases strongly with the incident angle compared with the cases of other pulses. Here the equivalent sheath width could be estimated to be $L_S=L_0/\cos\theta_I$, where L_0 is the sheath width measured at $\theta_I=0°$. The bias voltages on the reflector in this case are at floating potential. From these results we can say that the transmission coefficient for W_{TB} has strong dependence on the equivalent sheath width L_S, while other coefficients of W_T and W_R have weak dependences on the sheath width.

Figure 8 shows the velocity change of each pulse v_{TB}, v_R, or v_T as a function of the velocity of the incident pulse v_{IB}. Here, the data marked A show the case of an ion-beam velocity of 0, and, of course, W_{TB}, and so v_{TB}, do not appear in this case. The velocity of the transmitted beam component, v_{TB}, increases in proportion to the incident-beam velocity, v_{IB}. However, it becomes smaller than v_{IB} for larger values of v_{IB}, showing saturation

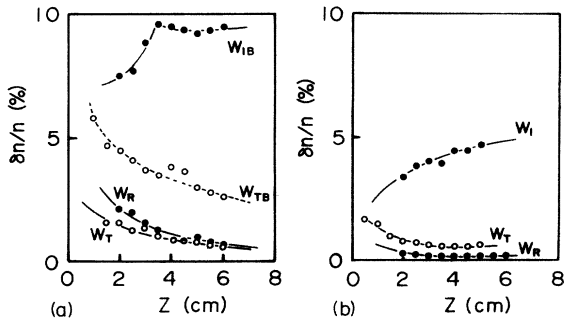

FIG. 4. Amplitude vs the position measured from the reflector in the (a) ion-beam system, and (b) the system without ion beam. $\theta_I=0°$, and V_b is the floating potential.

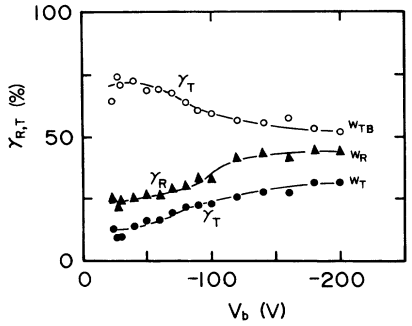

FIG. 5. Reflection and/or transmission coefficient vs the bias voltage on the reflector. Open circles stand for the transmission coefficient for the W_{TB}, closed circles for the transmission one for the W_T, and triangles for the reflection one for the W_R; $\theta_I=0°$.

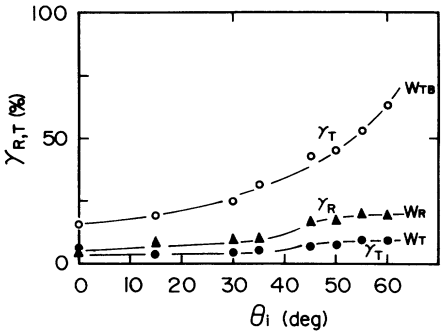

FIG. 7. Reflection coefficient for W_R, and transmission coefficient for W_{TB} and W_T vs the incident angle of the pulse. V_b is the floating potential.

characteristics. The velocity of the reflected pulse v_R and the transmitted one v_T are not influenced by v_{IB}, and are almost constant, although the velocity of the reflected pulse is slightly larger than that of the transmitted one.

The velocity ratio of each pulse to the incident pulse velocity is shown in Fig. 9 as a function of the sheath width. Here the velocities of the reflected pulse v_R corresponding to the pulse W_R of the transmitted beam v_{TB} to W_{TB}, and of the transmitted pulse v_T to W_T, are shown. The velocity ratio for v_{TB} and v_R increase slightly, while that of v_T decreases with the sheath thickness, where the incident angle $\theta_I=0°$ is kept constant. Here we varied bias voltages on the reflector V_b from -23 (floating potential) to -200 V in order to change the sheath thickness. It is reasonable to mention that the width of the sheath area becomes larger as the bias voltages on the reflector become more negative.

In earlier work [13,14], the "tunneling effect" of the electrostatic wave has been observed, but in the ion-beam mode no such phenomenon has been found so far. In the present investigation we have observed that the incident pulse propagates through the sheath area without time delay, such as the "tunnel effect" in the ion-beam mode, but the velocity $[v_{IB}=(1.6-2.2)C_s]$ of the incident pulse is smaller than what $[v_{IB}=(3.2-4.1)C_s]$ which is shown in the earlier work [13,14]. Consequently, time shifts $(\Delta\tau)$ between the incident pulse W_{IB} and the transmitted pulse W_{TB} are produced, and this difference becomes larger as the voltages on the reflector increase in negative side and/or the velocity v_{IB} of the incident pulse decreases. As soon as the incident pulse propagates through the opposite side of the sheath, it has been observed that the pulse splits into two pulses.

IV. DISCUSSION

A. Characteristics of each pulse

As seen from Fig. 5, the transmission coefficient of the transmitted pulse decreases as the bias voltage on the reflector becomes more negative. This phenomenon can be explained by taking into consideration the sheath thickness. Its thickness increases with negative bias voltages on the reflector, and as a result it is hard to propagate through the sheath area for the incident wave. Also,

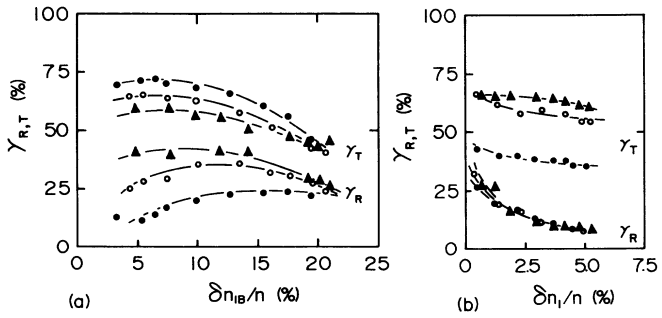

FIG. 6. Transmission and reflection coefficient vs the amplitude of the incident pulses. (a) Ion-beam system, $v_{IB}=6.3C_s$. (b) The system without ion beam, $v_I=C_s$ and $\theta_I=0°$. Closed circles to $V_b=-40$ V, open circles to $V_b=-80$ V, and triangles to $V_b=-120$ V.

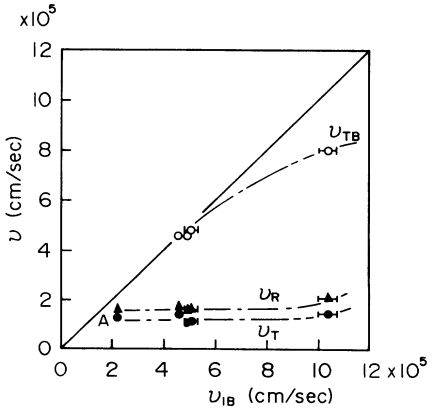

FIG. 8. Velocity change of the reflected pulse v_R and the transmitted pulse v_{TB} and v_T vs a function of the velocity of the incident pulse v_{IB}. V_b is the floating potential, and $\theta_I=0°$.

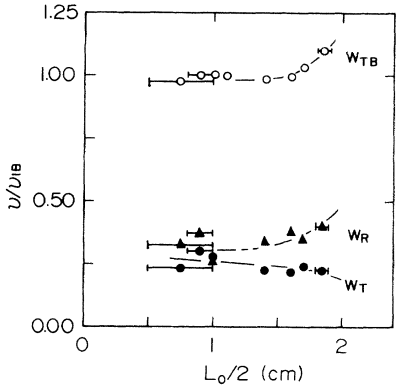

FIG. 9. Velocity ratio normalized by the incident pulse velocity vs the sheath width $L_0/2$; $\theta_I=0°$.

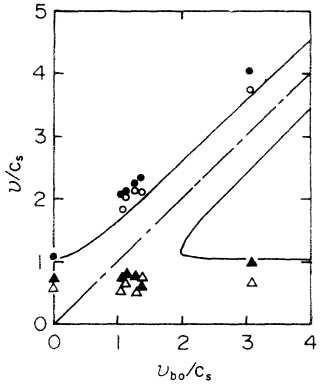

FIG. 10. Successive velocity change vs the ion-beam velocity. Closed circles refer to W_{IB}, open circles to W_{TB}, closed triangles to W_R, and open triangles to W_T. Solid lines represent the calculated results from Eq. (4) for $T=0.1$ and $\varepsilon=0.02$.

the ion beam hits the sheath edge to produce multiple pulses, and their amplitudes depend on the rate of the velocity change at the sheath edge.

Now let us discuss the characteristics of the pulses produced near the sheath edge by discussions in Refs. [18–20].

All the perturbation parts are set as follows:

$$f_1=|f_1|\exp\{i(kz-\omega t)\}\ , \tag{2}$$

and we assume the charge neutrality in the steady state is

$$n_{i0}+n_{b0}=n_{e0}\ , \tag{3}$$

where k is a wave number, ω is a frequency, and the equilibrium density n_{j0} ($j=i$, e, and b for ion, electron, and beam, respectively). From the equations of motion, continuity, and Poisson's equation,

$$y^2=1+T+\varepsilon\frac{2xy-x^2}{(y-x)^2-T}\ , \tag{4}$$

where, $x=v_{b0}/C_s=\sqrt{2\Delta V/T_e}$; ΔV is the voltage difference between the target and the driver plasma, $y=\omega/kC_s$, C_s is the ion-acoustic speed, $T=T_i/T_e$, T_i and T_e are ion and electron temperatures, respectively, $\varepsilon=n_{b0}/n_{e0}$, and $n=n_{e0}$ is the plasma density. Here we assumed that $\omega^2\ll(kv_{Te})^2$ and $(k_D/k)^2\gg1$, where v_{Te} is the electron thermal velocity and k_D is the Debye wave number. The results of the numerical calculations of Eq. (4) are shown in Fig. 10 for $T=0.1$ and $\varepsilon=0.02$. In this figure the experimental results are put together. From this figure, the incident and transmitted pulses (W_{IB}, and W_{TB}) could be identified as the fast ion-beam mode. However, the reflected pulse and the other transmitted pulse (W_R and W_T) are ion-acoustic modes, because their velocities are independent of the beam velocity.

B. Traveling time in the sheath area

Now we define the time δt, which is the necessary duration for a pulse going through two points, one located at the front (P_1) and the other at the back of the reflector (P_2), with a separation of 12 cm (see the inset in Fig. 11). The results of the variation of δt as a function of the incident angle θ_I is shown in Fig. 11. As seen from the results, δt decreases with the incident angle. Here the bias voltage on the reflector is at a floating potential throughout the experiments. From simple geometrical traces, the time duration δt required for the signal starting at position P_1 to reach P_2 may be given by the relation

$$\delta t=\frac{2L}{v_{IB}}+\frac{L_S}{v_S}=\frac{12}{v_{IB}}-\left[\frac{1}{v_{IB}}-\frac{1}{v_S}\right]\frac{L_0}{\cos\theta_I}\ , \tag{5}$$

where v_{IB} is the incident velocity of the signal in the uniform plasma, and v_S is that in the sheath area L_S. The numerical example is added to Fig. 11 by a solid line, where $v_S=10\times10^5$ cm/sec and $L_0\cong2.5$ cm are obtained from Figs. 3(a) and 3(b). As seen in the figure, experimental results are in good agreement with ones calculated in case (2), but those of case (1) do not agree. The reason for this is as follows: in case (1) the beam group B is reflected by the sheath in front of the reflector, and the amplitude

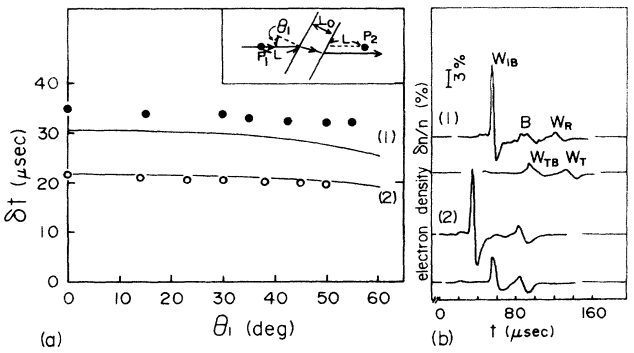

FIG. 11. (a) The change of the traveling time δt as a function of the incident angle θ_I. (b) Typical example of the wave pattern. The velocity of the pulse (1) is $v_{IB}=3.6\times10^5$ cm/sec, and that of (2) is $v_{IB}=4.9\times10^5$ cm/sec. B in the figure is the reflected beam. Solid lines are calculated from Eq. (5).

of the transmitted pulse decreases. The velocity v_{IB} of the incident pulse is smaller than that of the pulse in case (2), the velocity in this case being 4.9×10^5 cm/sec, while that in pulse (1) is 3.6×10^5 cm/sec.

C. Phase gap in the sheath area

Figure 12 shows the dependence of the time shift $\Delta\tau$ on the beam energy. Here $\Delta\tau$ has been defined in Figs. 3(b) and 3(c). In this case, the incident angle is $\theta_I=0°$ and the bias voltage on the reflector is at a floating potential. From this result, we can see that the time shift between two pulses decreases with the ion-beam energy. Consequently, the tunneling effect does not appear clearly for a high-energy ion-beam mode [13,14], but the pulse with small ion-beam energy shows clear evidence of the tunnel effect in the sheath area even in a beam mode. These phenomena can be understood by the following equation;

$$\Delta\tau=L_0\left[\frac{1}{v_{IB}}-\frac{1}{v_S}\right], \tag{6}$$

Here, the velocity of the pulses is given in Fig. 10 by the following relation:

$$v_{IB}\cong C_s+v_{b0}\quad (C_s<v_{b0}), \tag{7}$$

where $v_{b0}=2.19\sqrt{E}\times10^5$ cm/sec, E (eV) is the beam energy, and $C_s=2.04\times10^5$ cm/sec in the present parameters. The tunneling time and the width of the sheath area can be obtained from results in Figs. 3(a) and 3(b) as $L_0/v_S=2$–3 μsec and $L_0=2.5$ cm, respectively. These results are shown by the hatched area in Fig. 12. Reasonable agreement with experimental results can be seen.

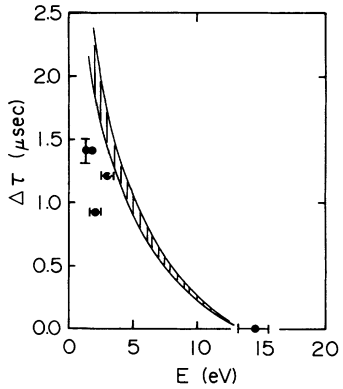

FIG. 12. Time shift $\Delta\tau$ between the incident W_{IB}, and transmitted pulse measured at the sheath area as a function of the beam energy E. Hatched area shows calculated results of Eq. (6). V_b is the floating potential, and $\theta_I=0°$.

V. CONCLUSION

The reflection and transmission of pulsive, large-amplitude ion-acoustic solitons have been investigated in the ion-beam mode. The incident soliton pulse is split into three pulses at the sheath area around the reflector electrode. These pulses are the fast ion-beam mode and two ion-acoustic modes. The incident pulse makes a time shift (phase gap) after traveling through a sheath area, and its shift increases as the beam energy becomes larger. This phenomenon can be interpreted by taking into consideration the beam velocity and the velocity in the sheath area. The numerical results show fairly good agreement.

ACKNOWLEDGMENT

The present work is supported in part by a Grant-in-Aid for Scientific Research from the Ministry of Education, Science, and Culture, Japan.

[1] S. Aksornkitti, H. C. Hsuan, K. E. Lonngren, and I. Alexeff, Phys. Fluids **11**, 1838 (1968).
[2] L. Schott, Phys. Lett. **89A**, 82 (1982); Phys. Fluids **26**, 3431 (1983).
[3] R. P. Dahiya, P. I. John, and Y. C. Saxena, Phys. Lett. **65A**, 323 (1978).
[4] O. Ishihara, I. Alexeff, H. J. Doucet, and W. D. Jones, Phys. Fluids **21**, 2211 (1978).
[5] Y. Nishida, Phys. Fluids **27**, 2176 (1984).
[6] G. Popa and M. Oertl, Phys. Lett. **98A**, 110 (1983).
[7] S. Raychaudhuri, B. Trieu, E. K. Thikis, and K. E. Lonngren, 1986 IEEE Trans. Plasma Sci. **14**, 42 (1986).
[8] E. F. Gabl and K. E. Lonngren, Plasma Phys. **26**, 799 (1984).
[9] Y. Nakamura, T. Ito, and K. Koga, Plasma Phys. **49**, 331 (1993).
[10] J. L. Cooney, M. T. Gavin, and K. E. Lonngren, Phys. Fluids B **3**, 2758 (1991).
[11] T. Nagasawa and Y. Nishida, Phys. Rev. Lett. **56**, 2688 (1986).
[12] T. Watanabe, Y. Kanamori, and N. Yajima, J. Phys. Soc. Jpn. **58**, 1273 (1989).
[13] Y. Nishida, K. Yoshida, and T. Nagasawa, Phys. Lett. A **131**, 437 (1988).
[14] Y. Nishida, K. Yoshida, and T. Nagasawa, Phys. Fluids B **5**, 722 (1993).
[15] T. Nagasawa, K. Yoshida, and Y. Nishida, in *International Conference on Plasma Physics, New Delhi, 1989,* edited by A. Sen and P. K. Kaw (New Delhi, 1989), Vol. 2, p. 713.
[16] T. Nagasawa and Y. Nishida, Phys. Lett. A **162**, 278 (1992).
[17] C. Matsuoka and N. Yajima, J. Phys. Soc. Jpn. **58**, 3939 (1989).
[18] Y. Kiwamoto, J. Phys. Soc. Jpn. **37**, 466 (1974).
[19] E. Okutsu, M. Nakamura, Y. Nakamura, and T. Itoh, Plasma Phys. **20**, 561 (1978).
[20] T. Nagasawa and Y. Nishida, Plasma Phys. **23**, 575 (1981).